Active structural vibration control using temperature constrained shape memory alloy actuation

G. Takács * **B. Rohaľ-Ilkiv** *

* *Slovak University of Technology*
Faculty of Mechanical Engineering
Institute of Automation, Measurement and Applied Informatics
(Tel: +421 2 5249 7193; e-mail: gergely.takacs@stuba.sk)

Abstract: This paper presents a modeling method for shape memory alloy-based actuators in vibration control and proposes a model predictive controller with separate deformation and thermal models to constrain temperatures levels in the actuator. A clamped cantilever beam equipped with actuators using pre-tensioned shape memory alloy wires is used as a demonstration device. The controller designed for this system aims to minimize beam tip deflections, while simultaneously constraining the input voltage of the actuators to limit values, in order to maximize the actuator efficiency. To solve this control problem, the paper proposes to use model predictive control with two separate models: one model for deformation dynamics and one for thermal dynamics. The deformation model is used in the cost function and input constraints, while predictions of the thermal model figure in the state constraints. The proposed first-principle models are identified based on experimental data and the input constrained model predictive control scheme is demonstrated in experiment with good results. The feasibility of the input and thermal constrained controller concept is estabilished in simulation.

Keywords: model predictive control, vibration control, shape memory alloy, linear systems

1. INTRODUCTION

Shape memory alloys (SMA) are materials with unidirectional cross-coupling between their thermal and mechanical response, caused by a solid-state phase-change at low temperatures. Thanks to this phase-change, a deformed SMA material will regain its original shape after heating above its transition temperature, which may be also induced by electrical Joule heating. Compared to traditional actuators, SMA exhibit some desirable properties; such as large force to mass ratio, light weight and large deformation amplitudes (Saito et al., 2011).

In addition to known medical uses, SMA actuators have been utilized in various applications; ranging from robotics to civil structures, and many others (Humbeeck, 1999). One of the major drawbacks of SMA actuators is that recoverable deformation amplitudes tend to diminish with increasing drive frequencies. Although some examples of employing SMA as actuating elements in active vibration control (AVC) are known in academic literature (Baz et al., 1990; Choi and Hwang, 2000), SMA are seldom used in AVC because of the aforementioned limitations.

Model predictive control (MPC) is a model- and optimization-based control algorithm known for its ability to explicitly handle process constraints (Rossiter, 2003; Maciejowski, 2000). These process constraints can be used to define a range of allowable temperatures for the SMA material, thereby maintaining the actuator near its phase-transition temperature. Natural (or forced) cooling of the SMA materials becomes less effective with higher dynamic drive frequencies, since the time for the material to cool is shortened. At higher drive frequencies—such as in vibration damping—instead of the expected oscillating motion, the SMA material will remain in a stable position, well over its phase-change temperature. Since the the deformation in SMA is directly related to temperature change, it is natural to assume that in order to increase the recoverable deformation amplitudes, one must operate close to the phase-change temperature.

This paper will introduce an SMA actuated vibration attenuation system for a clamped cantilever beam (Fig. 1(a)), using constrained model predictive control. A state-space model describing the input-output relationship between voltage input to the SMA actuator and deflection measured at the beam tip will serve as a basis to create sequences of state predictions. These state sequences are then used in a cost function, aimed at the minimization of deformation amplitudes. A second model representing the dynamics of the temperature change reacting to the input voltage supplied to the actuator will be used to generate a sequence of predictions augmenting the input constraints in the MPC control scheme.

1.1 Organization of this paper

The organization of this paper is as follows: the first section will introduce the experimental apparatus considered in this work. The second section is aimed at the theoretical basis of our discussion; introducing a mathematical model

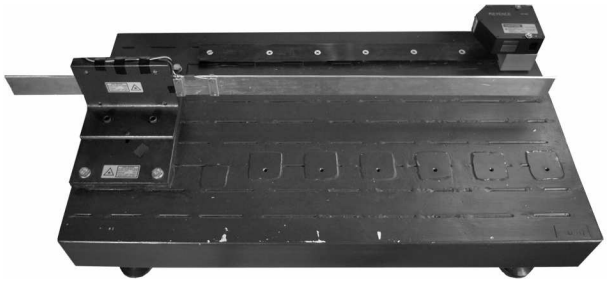

(a) Experimental apparatus — clamped cantilever beam

(b) Actuator prototype — front view

Fig. 1. The experimental apparatus is shown in (a) and the shape memory alloy actuator prototype is featured in (b)

for the deformation and thermal dynamics and the basics of model predictive control. This is followed by the system identification procedure and an experimental test with the MPC controller with input constraints. Section 5 will introduce the simulation results using an MPC controller augmented by thermal constraints and finally, Sect. 6 will conclude this paper.

2. LABORATORY INSTRUMENTATION

As illustrated in Fig.1(a), the experimental apparatus considered in this work consists of a clamped cantilever beam with SMA-based actuation and feedback control. Clamped cantilever beams are frequently used to model the vibration dynamics of lightly damped and under-actuated real-life systems in academic literature (Chiang and Safonov, 1991). Known applications include manipulators (Boscariol et al., 2010), helicopter rotors (Lu and Meng, 2006), aircraft wings (Amer and Bauomy, 2009), antenna systems, space structures and others.

The beam is made of EN AW 1050A aluminum material and measures 550×40×3 mm. Deformation is measured at the free end by a laser triangulation sensor (Keyence LK-G82), digitally processed and low-pass filtered (Keyence LK-G3001V) allowing through signals under 1000 Hz. The analysis of the basic vibration properties of the beam and initial control assessment was carried out in the ANSYS finite element modeling (FEM) environment (Takács and Rohaľ-Ilkiv, 2012; Trebuňa et al., 2011).

Actuation is provided by a SMA-based actuator prototype, shown on Fig.1(b). The actuator consists of two 0.5 mm diameter straight-annealed nickel-titanium SMA wires (MIDÉ Shape Memory Alloy Starter Kit) mounted on both sides of the beam at the clamped end. The length of the wires is 50 mm and they are placed in between conductive materials. The wires are connected to a simple rectifying circuit consisting of two diodes, separating the incoming signal to its positive and negative component. In case a sinusoidal signal is sent to the actuator, the positive half is allowed to flow to a wire on one side of the beam, while the negative to the other. The actuator prototype is connected to a general purpose amplifier (Bruel&Kjær Type 2718).

The feedback control system is implemented on a computer using the xPC Target rapid control prototyping platform containing a laboratory measurement card (National Instruments PCI-6030E) with analog inputs and outputs (National Instruments BNC-2111). The signal from the laser position sensor, voltage and current from the amplifier are connected to input channels, while the signal from the output channel is connected to the amplifier signal input. The simplified connection scheme of this experimental system is illustrated on Fig. 2.

3. THEORETICAL PREREQUISITES

The upcoming sections will introduce the theoretical basis on the model predictive control of the cantilever beam with AVC, using augmented constraints for thermal processes on the SMA actuator.

3.1 Continuous vibration and heat transfer dynamics

Assume that the vibration dynamics of the system can be approximated by the simple second order differential equation describing the motion of a point-mass with external force input (Benaroya and Nagurka, 2010):

$$m\ddot{q}(t) + b\dot{q}(t) + kq(t) = c_d u(t) \tag{1}$$

where m (kg) is the equivalent mass of the beam and the actuators, b (Ns/m) the equivalent viscous damping coefficient, k (N/m) the equivalent stiffness and let c_d (N/V) represent the scalar coefficient transforming input voltage potential to force $F(t) = c_d u(t)$ (N). We consider $u(t)$ (V) as input voltage and $q(t)$ (m) as deformation. If we choose position and velocity as state variables ($x_{d1}(t) = q(t), x_{d2}(t) = \dot{q}(t)$), it is possible to express this in a continuous, linear, time invariant state-space form:

$$\begin{bmatrix}\dot{x}_{d1}(t)\\ \dot{x}_{d2}(t)\end{bmatrix} = \begin{bmatrix}0 & 1\\ -\frac{b}{m} & -\frac{k}{m}\end{bmatrix}\begin{bmatrix}x_{d1}(t)\\ x_{d2}(t)\end{bmatrix} + \begin{bmatrix}0\\ \frac{c_d}{m}\end{bmatrix}u(t) \tag{2}$$

$$y_d(t) = [1\ 0]\begin{bmatrix}x_{d1}(t)\\ x_{d2}(t)\end{bmatrix} \tag{3}$$

where the output of the system is deformation $y_d(t) = q(t)$ (m) measured in a single point at the beam tip.

Assume that the temperature in the SMA wire is governed by simple electrical heating also known as Joule heating. If the wire is cooled only by convection, this heat transfer equation can be expressed by (Saito et al., 2011):

$$m_w c_p \dot{T}(t) = P(t) - h_c A_c T(t) \tag{4}$$

where m_w (kg) is the mass of the SMA wire, c_p (J/K) the specific heat of the wire material, h_c (J/m^{2}sK) is the heat convection coefficient and A_c (m^2) is the surface

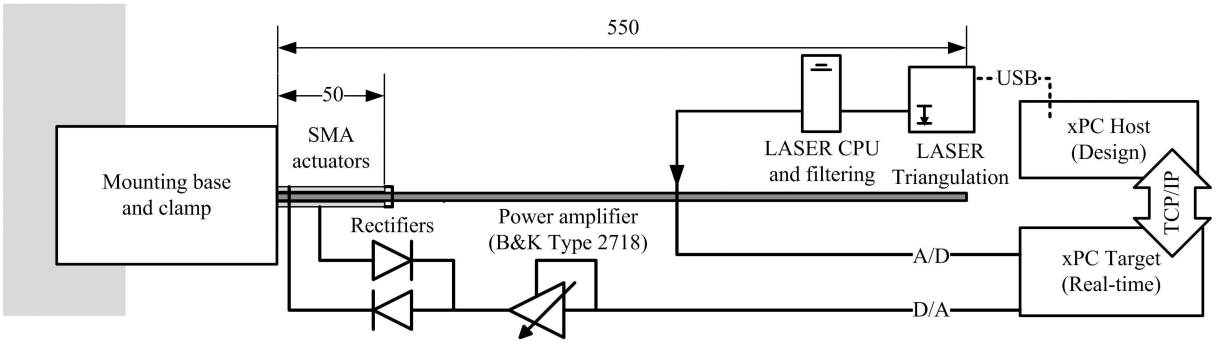

Fig. 2. Schematic representation of the experimental system

area of the heated wire. The power entering the system is represented by $P(t)$ (J/s,W) and the output here is the relative temperature difference $T(t)$ (K,^{o}C). To simplify the model, let us consider the resistance R (Ω) of the wire to be constant. The instantaneous power supplied to the wire can be expressed by $P(t) = U(t)I(t)$, which in the case of pure ohmic load is $P(t) = \frac{u(t)^2}{R}$; since in our case the voltage potential $U(t) = u(t)$ (V) is also the input to the deformation model. Differentiating this power gives $\dot{P}(t) = \frac{2}{R}u(t)$, which in combination with the heat transfer equation in (4) gives the following continuous state-space model:

$$\begin{bmatrix}\dot{x}_{t1}(t)\\ \dot{x}_{t2}(t)\end{bmatrix} = \begin{bmatrix}0 & 0\\ \frac{1}{m_w c_p} & -\frac{h_c A_c}{m_w c_p}\end{bmatrix}\begin{bmatrix}x_{t1}(t)\\ x_{t2}(t)\end{bmatrix} + \begin{bmatrix}\frac{2}{R}\\ 0\end{bmatrix} u(t) \quad (5)$$

$$y_t(t) = [0\ 1]\begin{bmatrix}x_{t1}(t)\\ x_{t2}(t)\end{bmatrix} \quad (6)$$

where the state $\boldsymbol{x}_t(t)$ contains power $x_{t1}(t) = P(t)$ and temperature $x_{t1}(t) = T(t)$ as variables. After choosing a suitable sampling time, both of these continuous models can be transformed into discrete equivalents (Franklin et al., 1997).

3.2 Prediction of future states based on discrete models

Let us assume that the dynamics of the controlled single-input single-output system can be described by the following discrete, linear, time-invariant state-space equation (Franklin et al., 1997):

$$\begin{aligned}\boldsymbol{x}_{d(k+1)} &= \boldsymbol{A}_d\boldsymbol{x}_{d(k)} + \boldsymbol{B}_d u_{(k)} \quad (7)\\ y_{d(k)} &= \boldsymbol{C}_d\boldsymbol{x}_{d(k)}\end{aligned}$$

where the subscript d (deformation) indicates that this is a model emulating the deformation of the cantilever beam. Similarly, the dynamics of the thermal response of the SMA wire can be described by a discrete LTI equation equivalent to Eqn. (7), where the variables and matrices are marked with the subscript t (thermal). Matrix $\boldsymbol{A}_d$ and $\boldsymbol{A}_t$ is a $\mathbb{R}^{2\times2}$ state matrix, $\boldsymbol{B}_d$ and $\boldsymbol{B}_t$ is a $\mathbb{R}^{2\times1}$ input matrix and $\boldsymbol{C}_d$ and $\boldsymbol{C}_t$ is $\in \mathbb{R}^{1\times2}$, while $\boldsymbol{D}_d$ and $\boldsymbol{D}_t$ representing direct input feed-through is omitted in this case. The dimension and structure of state variables $\boldsymbol{x}_{d(k)}, \boldsymbol{x}_{t(k)}$, outputs $y_{d(k)}, y_{t(k)}$ and the common input $u_{(k)}$ is equivalent to the continuous case presented previously.

Choosing a suitable discrete time horizon of n_p steps, we may predict the evolution of the future states—compactly expressed by $\overrightarrow{\boldsymbol{x}}_{d(k)}$ ($\overrightarrow{\boldsymbol{x}}_{t(k)}$)—based on the current state measurement $\boldsymbol{x}_{d0(k)}$ ($\boldsymbol{x}_{t0(k)}$) and the sequence of future inputs $\overrightarrow{\boldsymbol{u}}_{(k)}$, at time (k), for the deformation (thermal) model by recursive substitution of states (Maciejowski, 2000):

$$\begin{array}{lll} k & \boldsymbol{x}_{d(k)} & = \boldsymbol{x}_{d0(k)}\\ k+1 & \boldsymbol{x}_{d(k+1)} & = \boldsymbol{A}_d\boldsymbol{x}_{d(k)} + \boldsymbol{B}_d\boldsymbol{u}_{(k)}\\ k+2 & \boldsymbol{x}_{d(k+2)} & = \boldsymbol{A}_d\boldsymbol{x}_{d(k+1)} + \boldsymbol{B}_d\boldsymbol{u}_{(k+1)}\\ \vdots & \vdots & \\ k+n_p & \boldsymbol{x}_{d(k+n_p)} & = \boldsymbol{A}_d^{n_p}\boldsymbol{x}_{d(k)} + \boldsymbol{A}_d^{n_p-1}\boldsymbol{B}_d\boldsymbol{u}_{(k)} + \ldots\\ & & +\boldsymbol{A}_d\boldsymbol{B}_d\boldsymbol{u}_{(k+n_p)} + \boldsymbol{B}_d\boldsymbol{u}_{(k+n_p-1)}\end{array} \quad (8)$$

Note, that in the case of the thermal model one would use the matrices $\boldsymbol{A}_t$ and $\boldsymbol{B}_t$ instead. We may express this in a compact notation for both models by denoting (Maciejowski, 2000; Rossiter, 2003)

$$\overrightarrow{\boldsymbol{x}}_{d(k)} = \boldsymbol{M}_d\boldsymbol{x}_{d0(k)} + \boldsymbol{N}_d\overrightarrow{\boldsymbol{u}}_{(k)} \quad (9)$$

where matrices $\boldsymbol{M}_d$ and $\boldsymbol{N}_d$ are to be calculated according to (Rossiter, 2003)

$$\boldsymbol{M}_d = \begin{bmatrix}\boldsymbol{A}_d^0\\ \boldsymbol{A}_d^1\\ \vdots\\ \boldsymbol{A}_d^{n_p-1}\\ \boldsymbol{A}_d^{n_p}\end{bmatrix} \quad (10)$$

$$\boldsymbol{N}_d = \begin{bmatrix}\boldsymbol{0} & \boldsymbol{0} & \ldots & \boldsymbol{0} & \boldsymbol{0}\\ \boldsymbol{B}_d & \boldsymbol{0} & \ldots & \boldsymbol{0} & \boldsymbol{0}\\ \boldsymbol{A}_d\boldsymbol{B}_d & \boldsymbol{0} & \ldots & \boldsymbol{0} & \boldsymbol{0}\\ \vdots & \vdots & \ddots & \vdots & \vdots\\ \boldsymbol{A}_d^{n_p-1}\boldsymbol{B}_d & \boldsymbol{A}_d^{n_p-2}\boldsymbol{B}_d & \ldots & \boldsymbol{A}_d\boldsymbol{B}_d & \boldsymbol{B}_d\end{bmatrix} \quad (11)$$

Computing the state predictions in Eqn. (9) for the discrete thermal model involves the same procedure as presented previously and results in the prediction matrices $\boldsymbol{M}_t$ and $\boldsymbol{N}_t$, using the discrete state transition matrix $\boldsymbol{A}_t$ and input matrix $\boldsymbol{B}_t$ for the heat transfer model.

3.3 Cost function

Let us define a linear, quadratic cost function, expressing the contribution of future states $\overrightarrow{\boldsymbol{x}}_{d(k)}$ and future inputs $\overrightarrow{\boldsymbol{u}}_{(k)}$ into the scalar numerical control quality indicator J (-). This cost function uses the dual-mode paradigm, utilizing free control inputs for the first n_p steps and a

fixed matrix feedback controller afterwards (Scokaert and Rawlings, 1996):

$$J_k = \sum_{i=0}^{n_p-1} \left(\boldsymbol{x}_{d(k+i)}^T \boldsymbol{Q} \boldsymbol{x}_{d(k+i)} + u_{(k+i)}^T \boldsymbol{R} u_{(k+i)} \right) + \quad (12)$$
$$+ \boldsymbol{x}_{d(k+n_p)}^T \boldsymbol{P}_f \boldsymbol{x}_{d(k+n_p)}$$

where $\boldsymbol{Q} = \boldsymbol{Q}^T \geq 0$ is a user determined penalization matrix for states and $\boldsymbol{R} = \boldsymbol{R}^T \geq 0$ is a penalization matrix for inputs. Furthermore, $\boldsymbol{P}_f$ is the solution of the unconstrained, infinite-horizon quadratic regulation problem (Scokaert and Rawlings, 1996; Rossiter, 2003; Maciejowski, 2000):

$$\boldsymbol{P}_f - (\boldsymbol{A}_d + \boldsymbol{B}_d \boldsymbol{K})^T \boldsymbol{P}_f (\boldsymbol{A}_d + \boldsymbol{B}_d \boldsymbol{K}) = \quad (13)$$
$$= \boldsymbol{Q} + \boldsymbol{K}^T \boldsymbol{R} \boldsymbol{K}$$

where $\boldsymbol{K}$ is a fixed stabilizing feedback law (for example linear-quadratic (LQ)). The cost function in (12) can be compactly denoted as (Rossiter, 2003; Maciejowski, 2000)

$$J_k = \overrightarrow{\boldsymbol{u}}_{(k)}^T \boldsymbol{H} \overrightarrow{\boldsymbol{u}}_{(k)} + 2 \boldsymbol{x}_{d0(k)}^T \boldsymbol{G}^T \overrightarrow{\boldsymbol{u}}_{(k)} \quad (14)$$

Since the part $\boldsymbol{x}_{d0(k)}^T \boldsymbol{F} \boldsymbol{x}_{d0(k)}$ does not depend on the optimization variable $\overrightarrow{\boldsymbol{u}}_{(k)}$ and contributes only a fixed value to the cost at each iteration, we may omit it from the optimization procedure. In case we assume the model is fixed, $\boldsymbol{H}$ and $\boldsymbol{G}$ can be computed off-line by evaluating (Rossiter, 2003; Maciejowski, 2000)

$$\boldsymbol{H} = \sum_{i=0}^{n_p-1} \boldsymbol{N}_{d(i)}^T \boldsymbol{Q} \boldsymbol{N}_{d(i)} + \boldsymbol{N}_{d(n_p)}^T \boldsymbol{P}_f \boldsymbol{N}_{d(n_p)} + \mathcal{R} \quad (15)$$

$$\boldsymbol{G} = \sum_{i=0}^{n_p-1} \boldsymbol{N}_{d(i)}^T \boldsymbol{Q} \boldsymbol{M}_{d(i)} + \boldsymbol{N}_{d(n_p)}^T \boldsymbol{P}_f \boldsymbol{M}_{d(n_p)} \quad (16)$$

where (i) denotes the i-th block row, respectively (n_p) denotes the last block row of $\boldsymbol{N}_d$ and $\boldsymbol{M}_d$. Matrix $\mathcal{R}$ is a block matrix with the input penalty $\boldsymbol{R}$ on its main diagonal.

3.4 Constraints on voltage input and SMA temperature

Upper and lower constraints on all future input variables $\overrightarrow{\boldsymbol{u}}_{(k)}$ and states in the thermal model $\overrightarrow{\boldsymbol{x}}_{t(k)}$ can be expressed by (Maciejowski, 2000):

$$\underline{u} \leq \overrightarrow{\boldsymbol{u}}_{(k)} < \overline{u} \qquad \text{and} \qquad \underline{\boldsymbol{x}}_t \leq \overrightarrow{\boldsymbol{x}}_{t(k)} < \overline{\boldsymbol{x}}_t \quad (17)$$

This statement can be transformed to an equivalent form more suitable for online optimization (Maciejowski, 2000):

$$\begin{bmatrix} \boldsymbol{I} \\ -\boldsymbol{I} \end{bmatrix} \overrightarrow{\boldsymbol{u}}_{(k)} \leq \begin{bmatrix} \mathbf{1}\overline{u} \\ -\mathbf{1}\underline{u} \end{bmatrix}$$

and (18)

$$\begin{bmatrix} \boldsymbol{N}_{t(i)} \\ -\boldsymbol{N}_{t(i)} \end{bmatrix} \overrightarrow{\boldsymbol{u}}_{(k)} \leq \begin{bmatrix} \overline{\boldsymbol{x}}_t \\ -\underline{\boldsymbol{x}}_t \end{bmatrix} + \begin{bmatrix} -\boldsymbol{M}_{t(i)} \\ \boldsymbol{M}_{t(i)} \end{bmatrix} \boldsymbol{x}_{t0(k)}$$

where the equation on the left defines constraints on the allowable voltage potential to the system, while the equation on the right uses the predicted sequence of states based on the thermal model to define limits on the temperature in the wire (or in addition power as well). These two constraints are transformed in a compact notation to:

$$\begin{bmatrix} \boldsymbol{I} \\ -\boldsymbol{I} \\ \boldsymbol{N}_{t(i)} \\ -\boldsymbol{N}_{t(i)} \end{bmatrix} \overrightarrow{\boldsymbol{u}}_{(k)} \leq \begin{bmatrix} \mathbf{1}\overline{u} \\ -\mathbf{1}\underline{u} \\ \overline{\boldsymbol{x}}_t \\ -\underline{\boldsymbol{x}}_t \end{bmatrix} + \begin{bmatrix} 0 \\ 0 \\ -\boldsymbol{M}_{t(i)} \\ \boldsymbol{M}_{t(i)} \end{bmatrix} \boldsymbol{x}_{t0(k)} \quad (19)$$

3.5 The resulting MPC algorithm

The aim is to steer the state $\boldsymbol{x}_{d(k)}$ of the deformation model into the origin, essentially minimizing the deformation measured at the end of the vibrating beam. The cost function given by Eqn. (14) being minimized in this problem uses only the prediction matrices $\boldsymbol{M}_d$ and $\boldsymbol{N}_d$ belonging to the deformation model, requiring only the current deformation state $\boldsymbol{x}_{d(k)}$ at each sample. Constraining only the input $u_{(k)}$ creates a quadratic programming problem without considering the thermal properties of the wire. This formulation disregards the temperature constraints.

To add constraints for the allowable temperature range in the wire, one must create as second set of prediction matrices $\boldsymbol{M}_t$ and $\boldsymbol{N}_t$. These, however, do not contribute to the cost function as the minimization of the temperature is not desired in this case. Instead, the prediction matrices for the thermal model are used to augment the constraints with the temperature limits. Because the thermal model is expressed in the same optimization variable as the deformation model, the two interact with each other via the constraints. To evaluate the constraints, the current observed (measured) thermal state $\boldsymbol{x}_{t(k)}$ is required at each iteration.

In summary, the on-line MPC optimization problem involves minimizing the cost function with subject to the constraints on the voltage input and the predicted temperatures, implying the well-known constrained MPC algorithm (Rossiter, 2003; Maciejowski, 2000) augmented by the thermal model in the constraints:

Algorithm: Perform the following set of operations at each sampling instant:

- Observe (measure) actual system state at sample (k) for the deformation model $\boldsymbol{x}_{d(k)}$ and thermal model $\boldsymbol{x}_{t(k)}$.
- Minimize the MPC cost function (Rossiter, 2003; Maciejowski, 2000)

$$J_k = \sum_{i=0}^{n_p-1} \left(\boldsymbol{x}_{d(k+i)}^T \boldsymbol{Q} \boldsymbol{x}_{d(k+i)} + u_{(k+i)}^T \boldsymbol{R} u_{(k+i)} \right) +$$
$$+ \boldsymbol{x}_{d(k+n_p)}^T \boldsymbol{P}_f \boldsymbol{x}_{d(k+n_p)}$$

  subject to the following constraints

$$\overline{u} \leq u_{(k+i)} \leq \underline{u}, \qquad i = 0, 1, \ldots, n_p - 1 \tag{20}$$

$$\overline{\boldsymbol{x}}_t \leq \boldsymbol{x}_{t(k+i)} \leq \underline{\boldsymbol{x}}_t, \qquad i = 1, 2, \ldots, n_p - 1 \tag{21}$$

$$\boldsymbol{x}_{d(k+0)} = \boldsymbol{x}_{d(k)} \quad \text{(deform. state)} \tag{22}$$

$$\boldsymbol{x}_{t(k+0)} = \boldsymbol{x}_{t(k)} \quad \text{(thermal state)} \tag{23}$$

$$\boldsymbol{x}_{d(k+1)} = \boldsymbol{A}_d \boldsymbol{x}_{d(k)} + \boldsymbol{B}_d u_{(k)}, \quad i \geq 0 \tag{24}$$

$$y_{d(k)} = \boldsymbol{C}_d \boldsymbol{x}_{d(k)}, \quad i \geq 0 \tag{25}$$

$$\boldsymbol{x}_{t(k+1)} = \boldsymbol{A}_t \boldsymbol{x}_{t(k)} + \boldsymbol{B}_t u_{(k)}, \quad i \geq 0 \tag{26}$$

$$y_{t(k)} = \boldsymbol{C}_t \boldsymbol{x}_{t(k)}, \quad i \geq 0 \tag{27}$$

$$u_{(k+i)} = \boldsymbol{K} \boldsymbol{x}_{d(k+i)}, \quad i \geq n_p \tag{28}$$

- Apply the first element of the vector of optimal control moves $\overrightarrow{\boldsymbol{u}}_{(k)}$ to the controlled system, and restart the procedure.

4. EXPERIMENTAL WORK

4.1 System identification and model validation

The SMA actuator prototype was supplied a chirp signal with a 8 V peak amplitude, ranging from 1 Hz to 15 Hz in 300 s and sampled at a $T_s = 0.001$ s, to identify the parameters in the deflection model defined by Eqn. (2) and thermal model in Eqn. (5). In addition to the input signal, the voltage and current estimates were logged from the operational amplifier. The thermal profile of the SMA actuator was measured using a thermal camera (FLIR SC 660), and post-processed using proprietary software (FLIR ThermaCAM Researcher); see Fig. 3. The system identification procedure used the Matlab System Identification Toolbox (Ljung., 1999).

Two sets of deformation models were created from this data set: one with a $T_s = 0.001$ s sampling and free parameters for the experimental test without thermal constraints used in Sect. 4.2, and one with a $T_s = 0.01$ s sampling with a structure according to Eqn. (2) for the temperature-constrained version used in Sect. 5. The data set was pre-processed by removing means and trends. The data was re-sampled to $T_s = 0.01$ s for the structured model. Initial parameters were provided based on measurements, while the structure of the deformation model was also known. The parameters were identified using the iterative prediction-error minimization method (Ljung., 1999). The structured model is compared to the measured data set in Fig. 4(a).

After removing the outliers from the thermal data, it was re-sampled to $T_s = 0.01$ s. The model structure was set up according to Eqn. (5), while initial parameters were set based on material tables. The parameters for the thermal model were also identified using the iterative prediction-error minimization method (Ljung., 1999). The model is compared to the measured data set in Fig. 4(b). State Γ and input Ψ matrices for the continuous disturbance and thermal models were identified as:

$$\boldsymbol{\Gamma}_d = \begin{bmatrix} 0 & 1 \\ -2653 & -2.727\text{E}-1 \end{bmatrix} \qquad \boldsymbol{\Psi}_d = \begin{bmatrix} 0 \\ 8.979\text{E}-4 \end{bmatrix} \tag{29}$$

$$\boldsymbol{\Gamma}_t = \begin{bmatrix} 0 & 0 \\ 1.004 & -2.909\text{E}-2 \end{bmatrix} \qquad \boldsymbol{\Psi}_t = \begin{bmatrix} 1.830 \\ 0 \end{bmatrix}$$

4.2 MPC control without thermal constraints

An experimental verification test was devised to evaluate the damping effect of the SMA actuator prototype using the MPC algorithm on the cantilever beam. This test involved implementing a subspace identified, freely parameterized second order state-space system, modeling only the deformation dynamics of the controlled structure. The sampling time of the controller was identical to the sampling of the model, that is $T_s = 0.001$ s. The prediction horizon was set to $n_p = 10$ steps, the state penalization matrix was $\boldsymbol{Q} = \boldsymbol{C}_{\boldsymbol{d}}^{\boldsymbol{T}} \boldsymbol{C}_{\boldsymbol{d}}$ and the input penalization was set at $\boldsymbol{R} = 1\text{E}-4$ (-). The augmented constraints of Eqn. (19) are not utilized here, instead, only -7 (V) $\leq \overrightarrow{\boldsymbol{u}}_{(k)} < 7$ (V) symmetric input constraints are enforced. The controller algorithm was implemented in Simulink, utilizing the qpOASES quadratic programming solver (Ferreau et al., 2008).

The tip of the beam was deformed to a $y_{d(0)} = 6$ mm initial deflection as shown on Fig. 5(a), then it was allowed to settle in open- and closed-loop without further outside disturbance. The open-loop (free) response is compared to the MPC controlled response in Fig. 5(a), while the corresponding input signal $u_{(k)}$ is featured in Fig. 5(b). The effect of the closed-loop control with the SMA actuators is moderate, however, still faster than the open-loop response. The difference between the controlled and uncontrolled systems is the most obvious in the range

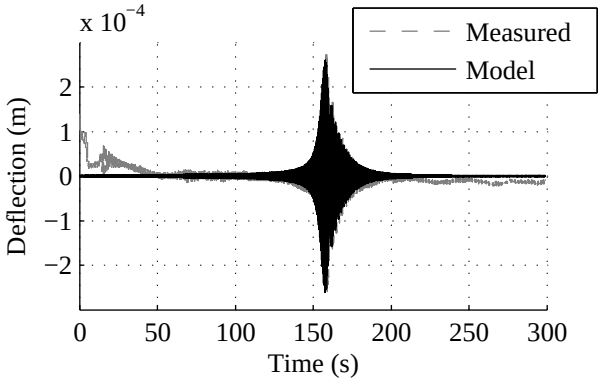

(a) Verification of the deformation model

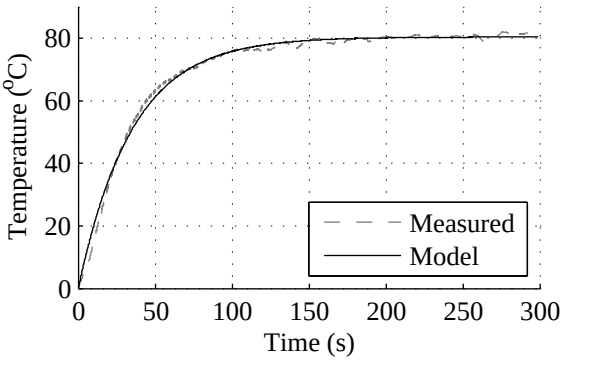

(b) Verification of the thermal model

Fig. 4. The deflection is contrasted to the modeled response in (a), while (a) shows the comparison of the measured and modeled temperature of the SMA wire (T_0 is ambient temperature.)

(a) Measuring the thermal response

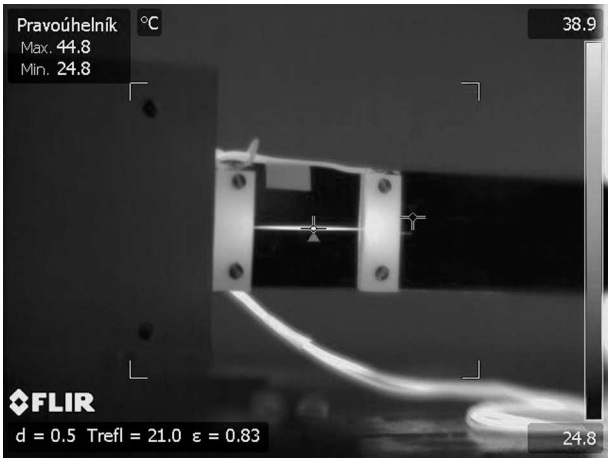

(b) Thermographic image of the actuator prototype

Fig. 3. The process of measuring the thermal response of the actuator is illustrated in (a), while the resulting thermographic image is shown in (b)

of small deformations (after 10–15 s), where the MPC controlled SMA actuator keeps the deformations near reference. The first half of the inputs are saturated, since the controller respects the input constraints. Later the constraints become inactive, but a certain level of control effort is still necessary to keep the output near reference.

5. SIMULATION STUDY

A simulation study designed to review the effects of MPC control with augmented thermal constraints was carried out using the deformation model and the heat-transfer model of the experimental structure. The MPC algorithm introduced in Sect. 3.5 was implemented in Matlab M-code, using the "quadprog" quadratic programming routine (MATLAB Optimization Toolbox) to minimize the cost function.

The simulated disturbance scenario was similar to the previously introduced experimental test, where the beam tip was deflected to a $y_{d(0)} = 5$ mm initial deformation and then left to vibrate without further simulated disturbances. The sampling time was set to $T_s = 0.01$ s, and the prediction matrices used in the cost ($\boldsymbol{M}_d$,$\boldsymbol{N}_d$) and constraints ($\boldsymbol{M}_t$,$\boldsymbol{N}_t$) were based on the discretized versions of the identified models featured in Eqn. (29). Prediction horizon was set to $n_p = 10$ steps, state penalization matrix was set to $\boldsymbol{Q} = \boldsymbol{C}_{\boldsymbol{d}}^{\boldsymbol{T}}\boldsymbol{C}_{\boldsymbol{d}}$ and the input penalization was set to a low value of $\boldsymbol{R} = 1\mathrm{E}-9$ (-). This configuration used the augmented constraints of Eqn. (19), implementing an input constraint of -8 (V) $\leq \overrightarrow{\boldsymbol{u}}_{(k)} < 8$ (V), a temperature constraint of 50 (^{o}C) $\leq \overrightarrow{\boldsymbol{T}}_{(k)} < 55$ (^{o}C) and an additional power estimate constraint of 0 (W) $\leq \overrightarrow{\boldsymbol{P}}_{(k)} < 1$ (W). In addition to the initial condition on the deformation, an initial temperature of $y_{t(0)} = 50$ ^{o}C is assumed.

The simulation results are graphically summarized in Fig. 6. The simulated open-loop response is contrasted to the simulated closed-loop response in Fig. 6(a), where it is clear that the results are very similar to the experimental measurements. While the effect of the actuators seems to be moderate, there is an improvement in the settling time, as it is the case with the physical system.

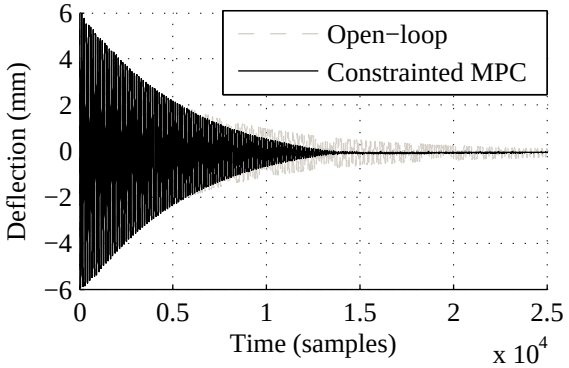

(a) Deflection output $y_{(k)}$ (mm)

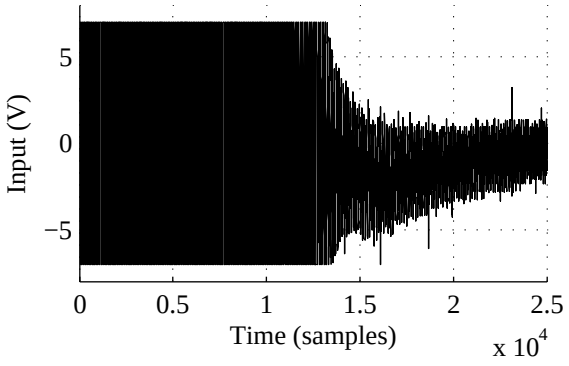

(b) Input voltage potential $u_{(k)}$ (V)

Fig. 5. The deflection measured at the beam tip under MPC control is contrasted to the open-loop response in (a), while the corresponding inputs are shown in (b)

Let us now comment on the effect of the temperature constraints, illustrated in Fig. 6(d). The temperature of the SMA wire in the actuator is initially rising, however, due to the effect of the augmented temperature constraint, later it is held at its allowable maximum value. Because the upper temperature constraint $\overline{x_{t2}} = \overline{T}$ becomes active, there must be a reduction in power. This power reduction

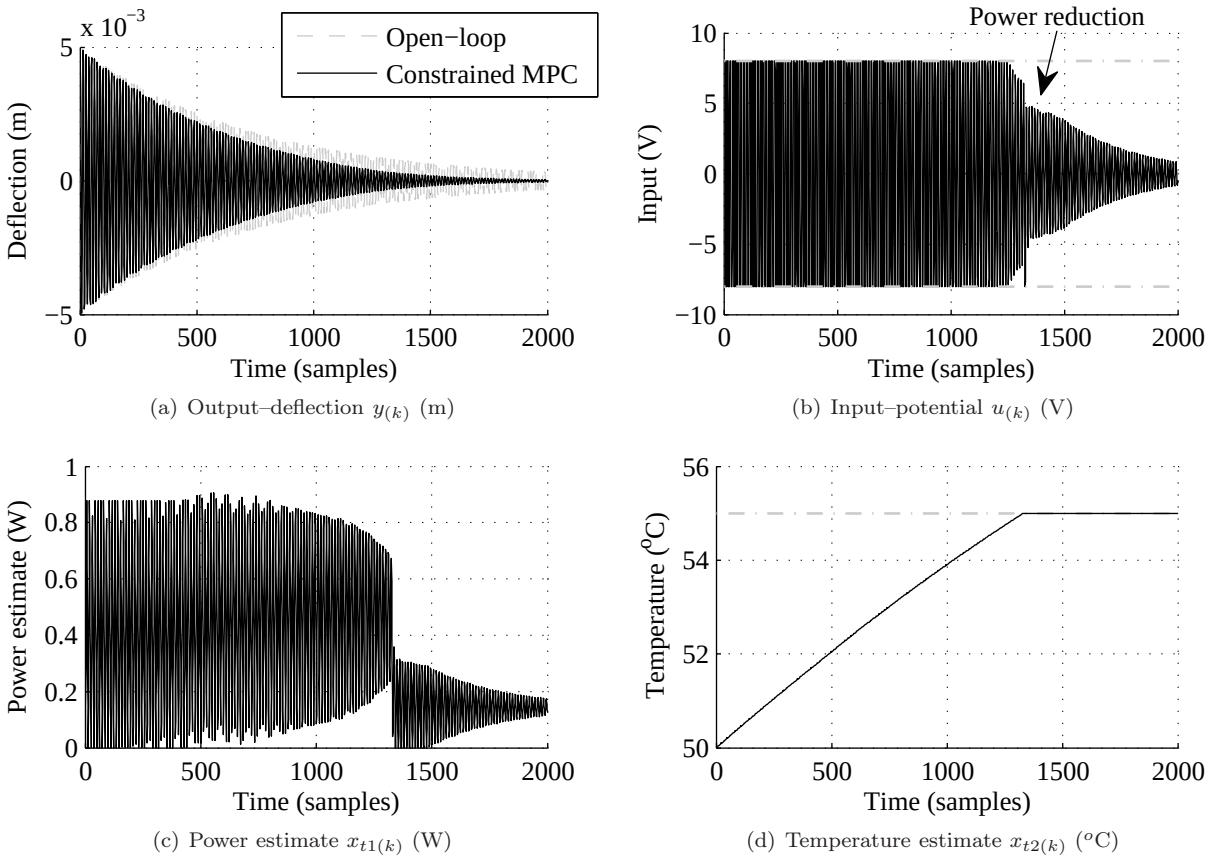

(a) Output–deflection $y_{(k)}$ (m)

(b) Input–potential $u_{(k)}$ (V)

(c) Power estimate $x_{t1(k)}$ (W)

(d) Temperature estimate $x_{t2(k)}$ (^{o}C)

Fig. 6. Simulation results for the SMA actuated model predictive vibration control system, augmented by constraints for future SMA wire temperatures

is clearly visible on the plot of estimated power in Fig. 6(c), where only the power compensating the effect of the convective cooling is allowed to enter the system. Only the lower power constraint $\underline{x_{t1}} = \underline{P}$ is active.

Even if the the thermal system indicates a reduction in power, this is not a manipulated variable. Instead, the two models are interconnected using the input variable $u_{(k)}$. The indicated power reduction then manifests itself on the inputs, as shown in Fig. 6(b). At first, the inputs are saturated because the controller respects the input constraints. Later these input constraints become inactive, however, the temperature constraints force the input to lower levels, resulting in a reduction of both power and temperature.

6. CONCLUSION

This work presented a smart memory alloy-based active vibration control system, with a closed-loop response governed by constrained model predictive control. Separate state-space models were developed for the deformation and heat-transfer dynamics of this active structure. A temperature constraint-augmented MPC controller has been proposed, which uses predictions of the deformation model in the cost function, while respecting thermal limitations by a separate prediction model in the constraints.

The experiment verifying the effect of the SMA actuator using an MPC algorithm with input constraints resulted in improved settling times, mainly in the range of small deformations. Due to the physical limitations of the actuator, the overall damping effect was moderate. The results of the simulations implementing the MPC algorithm with temperature constraints demonstrated a scenario, where the input was manipulated in a way to keep the temperature in the SMA material between prescribed limits, while minimizing the deformations as well. Although the electric power is not a direct manipulated variable in this setup, the dynamics of the deformation and thermal models are interacting through the common voltage input variable.

The proposed method may be used to set thermal limits on the SMA material that will maintain the actuator around its phase-change temperature. Using the SMA actuator only near its phase-change region may potentially increase its deformation range, to achieve higher than usual deformation amplitudes at drive frequencies that are suitable for the vibration control of lightly damped structures.

Future work shall verify the proposed algorithm in experiment, and test whether maintaining the SMA material around phase-transition temperatures can increase deformation amplitudes in dynamic drive modes. A better mathematical representation is required to model the transition between the voltage input to the actuators and the power in the thermal system. The development of an alternative state-space model is planned, where temperature will be directly influencing the mechanical behavior—as is the case for the real physics. A more elaborate actuator

prototype is planned to increase the damping effect in closed-loop control.

ACKNOWLEDGEMENTS

The authors would like to thank the financial support granted by the Slovak Research and Development Agency (SRDA) provided under the contracts APVV 0910-10, APVV 0280-06 and APVV 0131-10.

REFERENCES

Amer, Y. and Bauomy, H. (2009). Vibration reduction in a 2DOF twin-tail system to parametric excitations. *Communications in Nonlinear Science and Numerical Simulation*, 14(2), 560 – 573. doi:10.1016/j.cnsns.2007.10.005.

Baz, A., Imam, K., and McCoy, J. (1990). Active vibration control of flexible beams using shape memory actuators. *Journal of Sound and Vibration*, 140(3), 437 – 456. doi:10.1016/0022-460X(90)90760-W.

Benaroya, H. and Nagurka, M.L. (2010). *Mechanical Vibration: Analysis, Uncertainities and Control*. CRC Press, Taylor&Francis Group, Boca Raton, Florida, 3. edition.

Boscariol, P., Gasparetto, A., and Zanotto, V. (2010). Model predictive control of a flexible links mechanism. *Journal of Intelligent Robotic Systems*, 58, 125–147. URL http://dx.doi.org/10.1007/s10846-009-9347-5. 10.1007/s10846-009-9347-5.

Chiang, R.Y. and Safonov, M.G. (1991). Design of $\mathcal{H}_\infty$ controller for a lightly damped system using a bilinear pole shifting transform. In *American Control Conference, 1991*, 1927 –1928.

Choi, S.B. and Hwang, J.H. (2000). Structural vibration control using shape memory actuators. *Journal of Sound and Vibration*, 231(4), 1168 – 1174. doi:10.1006/jsvi.1999.2637.

Ferreau, H.J., Bock, H.G., and Diehl, M. (2008). An online active set strategy to overcome the limitations of explicit MPC. *International Journal of Robust and Nonlinear Control*, 18(8), 816–830.

Franklin, G.F., Powell, J.D., and Workman, M.L. (1997). *Digital Control of Dynamic Systems*. Addison-Wesley, Boston, Massachusetts, United States of America, 3. edition.

Humbeeck, J.V. (1999). Non-medical applications of shape memory alloys. *Materials Science and Engineering: A*, 273–275(0), 134–148. doi:10.1016/S0921-5093(99)00293-2.

Ljung., L. (1999). *System Identification: Theory for the User*. PTR Prentice Hall, Upper Saddle River, NJ., 2. edition.

Lu, H. and Meng, G. (2006). An experimental and analytical investigation of the dynamic characteristics of a flexible sandwich plate filled with electrorheological fluid. *The International Journal of Advanced Manufacturing Technology*, 28, 1049–1055. URL http://dx.doi.org/10.1007/s00170-004-2433-8. 10.1007/s00170-004-2433-8.

Maciejowski, J.M. (2000). *Predictive Control with Constraints*. Prentice Hall, Upper Saddle River, New Jersey, 1. edition.

Rossiter, J.A. (2003). *Model-Based Predictive Control: A Practical Approach*. CRC Press, Boca Raton, Florida, 1. edition.

Saito, S., Deng, M., Jiang, C., and Minami, M. (2011). Operator based design for vibration control of flexible arm using sma actuator with hysteresis. In *Modelling, Identification and Control (ICMIC), Proceedings of 2011 International Conference on*, 145 –150. doi:10.1109/ICMIC.2011.5973691.

Scokaert, P.O.M. and Rawlings, J.B. (1996). Infinite horizon linear quadratic control with constraints. In *Proceedings of IFAC'96 World Congress*, volume 7a-04 1, 109–114. San Francisco, United States of America.

Takács, G. and Rohaľ-Ilkiv, B. (2012). *Predictive Vibration Control: Efficient constrained MPC vibration control for lightly damped mechanical systems*. Springer, London, United Kingdom, 1. edition. doi:10.1007/978-1-4471-2333-0.

Trebuňa, F., Frankovský, P., Guľa, M., and Hudăk, P. (2011). Numerically computed dynamics rotor using ANSYS software. In *Proceedings of the 4th international conference MMaMS 2011: Modelling of Mechanical and Mechatronical Systems*. Herľany, Slovakia.